

# Efficiency of Energy Harvesting in Ni–Mn–Ga Shape Memory Alloys

Paul Lindquist<sup>1</sup> · Tony Hobza<sup>1,3</sup> · Charles Patrick<sup>1,2,4</sup> · Peter Müllner<sup>1</sup>

Published online: 5 March 2018 © ASM International 2018

**Abstract** Many researchers have reported on the voltage and power generated while energy harvesting using Ni-Mn-Ga shape memory alloys; few researchers report on the power conversion efficiency of energy harvesting. We measured the magneto-mechanical behavior and energy harvesting of Ni-Mn-Ga shape memory alloys to quantify the efficiency of energy harvesting using the inverse magneto-plastic effect. At low frequencies, less than 150 Hz, the power conversion efficiency is less than 0.1%. Power conversion efficiency increases with (i) increasing actuation frequency, (ii) increasing actuation stroke, and (iii) decreasing twinning stress. Extrapolating the results of low-frequency experiments to the kHz actuation regime yields a power conversion factor of about 20% for 3 kHz actuation frequency, 7% actuation strain, and 0.05 MPa twinning stress.

**Keywords** NiMnGa · Magnetic shape memory · Mechanical behavior · Energy harvesting · Efficiency · Inverse magneto-plastic effect

- Micron School of Materials Science and Engineering, Boise State University, Boise, ID, USA
- Department of Electrical and Computer Engineering, Boise State University, Boise, ID, USA
- <sup>3</sup> Present Address: SpaceX Corporation, Hawthorne, CA, USA
- Present Address: Department of Electrical Engineering, Princeton University, Princeton, NJ, USA

## Introduction

Generating power from ferromagnetic shape memory alloys relies on uniaxial compressive loading and unloading a single crystal while working against a magnetic field perpendicular to the load axis. During loading, twin boundary motion leads to a reorientation of the crystallographic c direction, which coincides with the direction of easy magnetization. During unloading, the bias magnetic field restores the sample deformation and the direction of the sample magnetization via twin boundary motion in the reverse direction. The change in magnetization induces an electromotive force,  $\varepsilon$ , in a pickup coil wrapped around the crystal by Faraday's law of magnetism,

$$\varepsilon = -N \frac{\partial \Phi}{\partial t},\tag{1}$$

where N is the number of conductor turns,  $\phi = A\vec{B}$  with the area of the coil A and magnetic field or magnetic flux density  $\vec{B}$ . Harvesting power in this way is referred to the inverse magneto-plastic (IMP) effect [1, 2].

Magnetic shape memory alloys are viable candidates for power generation at high frequencies, because they deform and recover large strains (6–10%) while simultaneously changing internal magnetization, twin boundaries move at high velocities [3], the stresses for twin boundary motion are low [4], and there is magnetically coupled shape anisotropy with the twin boundary motion [5]. Moving twin boundaries quickly changes the internal magnetization and results in generating a high voltage in a pickup coil. Suorsa et al., found that mechanically pulsed twin boundaries moving at 1.9 m/s generates a peak voltage of 85 V in a 4000 turn pickup coil wound about a ferromagnetic core to increase the coils output [1].



Paul Lindquist paullindquist@boisestate.edu

Adopting the experimental setup described by Karaman et al., Bruno et al., Nelson et al., Guiel et al., and Carpenter et al. studied energy harvesting of Ni-Mn-Ga single crystals between 1 and 75 Hz with peak-to-peak strain between 3 and 6% and bias magnetic fields optimized near 0.6-0.7 T [6-9]. The focus of these works was to model the martensite reorientation and maximize the power output of the pickup coil. Bruno et al. reported a maximum peak-topeak voltage of 0.95 V when the peak-to-peak strain was 5% at 75 Hz. Nelson et al. found that moving the bias magnetic field 12° off the orthogonal to the load axis increased the peak-to-peak voltage to 0.55 V at 20 Hz and 5% strain. Continuing with Nelson's research, Guiel et al. found similar results for the peak-to-peak coil voltage. They also reported a peak power output of 10 µW at 3% peak-to-peak strain when the 0.5 T bias magnetic was 37° off axis while testing at 20 Hz. Peak-to-peak voltages reported by Guiel et al. [9]. and Nelson et al. [8]. are much lower than that reported by Suorsa et al. [1]., 0.55 V compared to 85 V. The voltages are low because the maximum twin boundary velocity was constrained by the cyclic loading test system, the pickup coil was not coupled with a core, and the number of pickup windings was four times less.

Increasing the induced voltage and power generated seems to be the main focus so far; not reported in any of these studies was the efficiency of energy harvesting, the ratio of the electrical work density to the mechanical work density. From Bruno et al., the stress hysteresis of their sample while cycling at 20 Hz was approximately 1.5 MPa; with a peak-to-peak strain of 0.04, we estimate a 60 kJ/m<sup>3</sup> mechanical work density. Moreover, from the results reported by Guiel et al., from a peak power of 10 μW, we estimate an electrical power density of 70 J/m<sup>3</sup> at 20 Hz and a strain of 0.04. Combining these results, we compute an energy harvesting efficiency of 0.1%. Additional work is needed to understand the interplay between electrical output work density and mechanical input work density and factors that increase the energy harvesting efficiency.

In this study, an instrumented test apparatus was used to investigate the power generated as a function of frequency from 25 to 150 Hz, magnetic field strength 0.1–0.8 T (0.08–0.64 MA/m), and peak-to-peak strain from 0.5 to 2.5%. The system consisted of a load frame, a load cell, a displacement transducer, an electrical pickup coil, a linear voice coil motor and an adjustable electromagnet. This apparatus measured stress, strain and power generation while cyclically loading the crystal in displacement control at various test frequencies. From these results, we report mechanical work density, electrical work density and the efficiency of transforming mechanical work into electrical work.



The Magneto-Mechanical Test Apparatus (MMTA) shown in Fig. 1 measures stress, strain and electrical work from a pickup coil surrounding the test sample [10, 11]. The MMTA system consists of: (a) an electromagnet with 20 mm pole pieces set up for magnetic fields between 0 and 0.8 T (0-0.64 MA/m), Model 3470, GMW Associates, San Carlos, CA; (b) a voice coil linear motor with a magneto-force 80 N at 100% duty cycle and 240 N at 10% duty cycle, Model NCM05-28-180, H2W Tech, Santa Clarita, CA; (c) an LVDT displacement transducer, Model MHR-010, Measurement Specialties, Hampton, VA, with a custom-made signal conditioning module scaled to output  $\pm$  300  $\mu$ m displacement using an LVDT signal conditioning IC, AD 698 IC, Analog Devices, Norwood, MA [12]; (d) a sample compression micrometer, Model BM30-10 0-10 mm travel micrometer, 0.01 mm/div, Newport Corp., Irvine, CA; (e) A 44 N piezoelectric load cell, Model 208-C01, PCB Piezotronics Inc., Depew, NY; (f) and interchangeable die springs, with spring constants of 135, 269, and 461 N/mm that varied the resonant frequency of the linear voice coil motor, Century Springs Inc, Los Angeles, CA; (g) a single crystal Ni-Mn-Ga test sample, (h) 1601 turn 43 AWG pickup coil that surrounds the test sample.

The pickup coil was wound on a modified sewing machine bobbin winder (AlphaSew P60999NS Portable Bobbin Winder, Los Angeles, CA) using 0.0031 mm<sup>2</sup> of insulated copper wire (43 AWG polycoated pickup wire, Stewart-MacDonald, Athens, OH) and a machinable wax bobbin (Freeman Manufacturing and Supply, Avon, OH) yielding a coil with an inner diameter of 6.2 mm by 11 mm long. A counter and a servomotor to control the wire feed to the bobbin was added to it. During

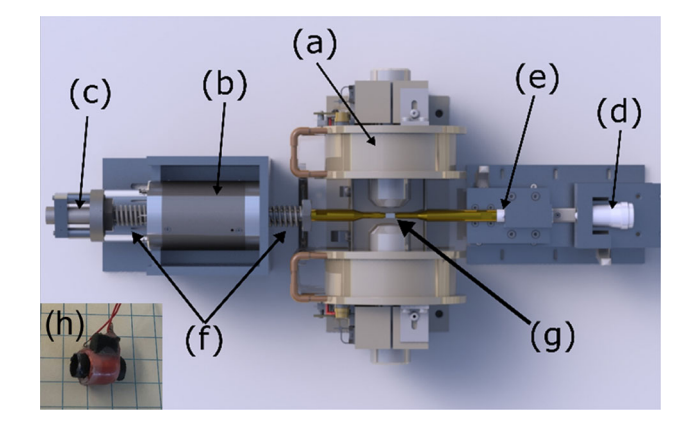


**Fig. 1** Magneto-mechanical test apparatus (MMTA) with a variable-field electromagnet (*a*), voice coil motor (*b*), linear-variable differential transformer (*c*), micrometer (*d*), piezoelectric force transducer (*e*), springs to tune the resonant frequency of the motor (*f*), Ni-Mn-Ga specimen (*g*), and 1601 winding, 11 mm long pickup coil (*h*)



winding, cyanoacrylate glue was applied to the windings to glue them together. Afterward, the wax bobbin was melted away to finish the pickup coil; Fig. 1h. To get maximum power transfer, a 290  $\Omega$  load resistor was connected across the pickup coil leads, and the load resistor was matched to the coil impedance. In the MMTA, the sample was placed inside the pickup coil where the coil axis was oriented perpendicular to the bias magnetic field. The electromotive force,  $\epsilon$ , induced in the pickup coil was measured with a variable gain, 1 to 50X, op amp that buffered the 1601 turn coil output from the analog to digital converter (ADC) input.

A single crystal of Ni<sub>51.6</sub>Mn<sub>26.3</sub>Ga<sub>22.1</sub> grown by the Bridgman-Stockbarger technique using the crystal growth system developed by Kellis et al. [13], was aligned with an X-ray diffractometer such that the {100} faces of the crystal matched those surfaces to be cut. Prior to cutting the samples, the single crystal was characterized for composition along the crystal axis of growth by an SEM (Hitachi S-3400 N) fitted with an energy-dispersive spectrometer. The composition varied from the seed end to the top of the crystal with the composition gradient for Mn and Ni greatest at 20-50 mm from the seed end. The crystal was also scanned along the crystal axis by X-ray diffraction (Bruker D8 Discovery) to determine how the crystal structure varied along the axis of growth. The region near the seed had 10 M crystal structure that slowly changed to 14 M, finally changing to non-modulated NM crystal structure farthest from the seed. The sample was cut from the end nearest the seed, 0-7 mm, it had the 10 M crystal structure and a composition of Ni  $51.3 \pm 0.2$ , Mn  $26.3 \pm 0.4$  and Ga  $22.4 \pm 0.4$  atomic percent. A wire saw was used to cut parallel to {100} faces of the crystal. All faces of the sample were polished with 1 µm diamond paste, yielding a crystal  $6.46 \times 2.08 \times 3.84 \text{ mm}^3$ . Finally, the transformation temperatures of the sample were measured at a low magnetic field (250 Oe) in a vibrating sample magnetometer (MicroSense Model 10 VSM) while heating and cooling a cryostat from -65 to  $150^{\circ}$  C. The transformation temperatures were  $M_s = 38$ ,  $M_f = 30$ ,  $A_{s-1}$ = 38 and  $A_f = 45$  °C.

When the sample was poled with the magnetic field, the *c*-axis aligned with the magnetic pole pieces of the MMTA and the (100) and (010) aligned with the other faces of the polished crystal. To obtain the stress–strain response without a magnetic field, the sample was tested under compression in a screw-driven mechanical test system Zwick-1445 (Zwick, Ulm). Magneto-stress strain measurements at 0.0, 0.2, 0.4 and 0.6 T (0.16, 0.32 and 0.48 MA/m) were obtained in the MMTA by compressing the sample with the sample compression micrometer against a set of compliant springs with the electromagnet on. Stress was computed by measuring the spring deflection with the

LVDT displacement gauge times the spring constant divided by the sample cross-sectional area and strain was computed by taking the difference of the total compression as read on the compression micrometer minus the spring deflection divided by the sample length.

This system was capable of dynamic magneto-mechanical testing from 10 to 300 Hz when the voice coil motor was cycled to load and unload the sample with the magnetic field-biased perpendicular to the load axis. A proportional, integral, and derivative (PID) control program written in Simulink was used to run in displacement control, from 10 to 300 µm peak-to-peak displacement during testing at various frequencies and magnetic flux density. Analog inputs for force, displacement, and power supply monitoring were connected to a multiplexed fourchannel 16-bit analog to digital converter (ADC). The current to the electromagnet was controlled by analog output from a 16-bit digital to analog converter (DAC) connected to the remote input on a (60 V and 10A) programmable power supply, Ametek Model DLM 600, San Diego, CA. The ADC and DAC inputs and outputs were controlled by an embedded controller board inside a personal computer, Model ACE 1104 Power PC, dSpace Inc., Wixom, MI. The embedded controller was programmed from scripts written in MatLab along with a symbolic model for the ADC and DAC converters written in Simulink, an accessory software package from MathWorks, Natick, MA. The MatLab/Simulink software was crosscompiled and linked into embedded code that was downloaded to the dSpace controller card.

The Ni-Mn-Ga crystal was glued with cyanoacrylate adhesive to a brass platen 4.5 mm in diameter and it was centered between the pole pieces of the magnet. Before testing, the magnetic field on the sample was ramped to 0.61 T (0.48 MA/m) without constraint from the opposite brass platen and the sample expanded to the maximum length. The magnetic field of 0.61 T was selected based on a series of experiments at 25, 50, 75 and 100 Hz with magnetic field ranging from 0.3 to 0.8 T (0.24–0.64 MA/m) that determined the maximum power conversion efficiency; Fig. 2. Power was harvested from an induction coil placed around the sample with a 290  $\Omega$  load resistor shunted across the coil leads. The testing sequence was: (1) compress the sample to 3% strain with the sample compression micrometer; (2) start the dSpace control and data collection program; (3) set the magnetic field to the bias electromagnet to 0.61T; (4) set the voice coil motor to run at the lowest peak-to-peak displacement; (5) adjust the gain on the voice coil amplifier from zero to the gain needed to achieve the peak-to-peak displacement; (6) start and stop data capture to acquire 28,000 data points; (7) step to the next peak-to-peak displacement increment acquiring data for 15, 30, 45, 60, 75, 100, 125, and 150 μm by repeating



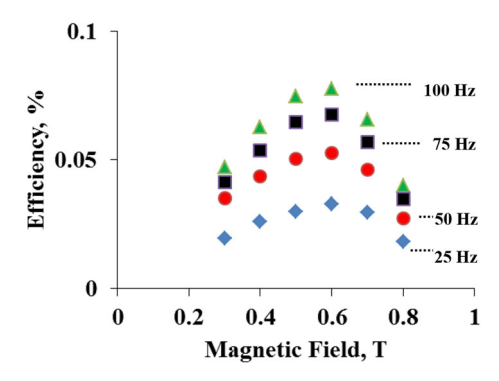


**Fig. 2** Power conversion efficiency measured at 25–100 Hz while varying the field from 0.3 to 0.8 T at constant peak-to-peak strain at 0.36%. All other experiments were run at 0.61 T flux densities

steps 6 and 7 until complete; (8) repeat steps 4 through 7 increasing by 25 Hz from 25 to 150 Hz. During step (5), the motor continually oscillates until the feedback reaches each peak-to-peak displacement step. The motor and magnetic fields are turned off when changing the oscillation frequency, but the initial 3% compression strain of the sample was not changed. For each test, analog inputs for force, displacement, pickup coil, electromagnet voltage and electromagnet current were sampled simultaneously with a 16-bit ADC channel every 0.05 ms, 28,000 data points per test. The dSpace ControlDesk computer program handles data acquisition and saves the data to disk for further data analysis.

Raw data from the dSpace ControlDesk were analyzed and graphed in MatLab and MicroSoft Excel. Figure 3 is an example of inputs from the force, displacement and pickup coil that varied during each cycle of the experiment. The displacement signal was sine function (Fig. 3, bottom curve) except for the lowest frequency (25 Hz), for which the displacement function had plateaus for minimum and maximum values. Stress and strain was computed from the sample dimensions and the load cell force signal along with the LVDT displacement signal for each of the timestamped data points. For each cycle, the raw data were averaged by using a peak-finding algorithm that found the major peak in each cycle, algorithm from MatLab. Once the major peak for each cycle was found, the data were synchronized and averaged on a point-by-point basis. There were 28,000 data points per test, at 100 Hz and 0.005 ms per sample this amounts to 200 samples per cycle and the ability to average over 140 cycles.

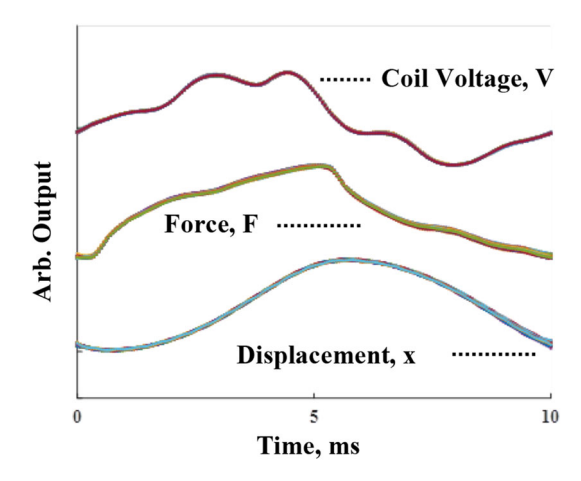


**Fig. 3** Typical output from the load cell, the LVDT displacement transducer, and the pickup coil for 136 cycles overlaid at 0.024 peak-to-peak strain and 100 Hz. Data normalized and shifted along the y-axis

The mechanical work density,  $W_{\text{mechanical}}$ , per cycle (units J/m<sup>3</sup>) was computed by integrating the cyclic stress versus strain curves using the trapezoidal rule:

$$W_{mechanical} = \int_0^{\epsilon_{\text{max}}} \sigma(\epsilon) d\epsilon - \int_{\epsilon_{\text{max}}}^0 \sigma(\epsilon) d\epsilon.$$
 (2)

The electrical work output per cycle,  $W_e$ , was the power output from the coil,  $\varepsilon^2/R$ , integrated over the time for one compression and expansion cycle, (units J).

$$W_e = \int_0^T \varepsilon^2(t) / R dt, \tag{3}$$

where T is the period of actuation,  $\varepsilon$  is the electromotive force and R is the load resistor. To calculate the electrical work density,  $W_{\rm electrical}$  (units J/m³),  $W_{\rm e}$  was divided by the sample volume. To compare results to other research, the peak-to-peak voltage and the root mean square of the pickup coil voltage was computed.

# Results

The piezoelectric load cell measured dynamic force changes very well, but did not record the static force. Using the techniques described earlier, the magneto-stress was measured by slowly compressing the sample from 0 to 5% strain while holding the magnetic field constant. The magneto-stress was measured at magnetic fields of 0.0, 0.2, 0.4 and 0.6 T, Fig. 4a. The twinning stress without magnetic field was 0.5 MPa. The magneto-stress increased with increasing compressive strain when the magnetic field was on. Testing was started by compressing the sample 3% at magnetic field of 0.6 T. During each experiment, for all frequencies there was little or no drift of the output signal from the dynamic load cell or the displacement transducer;



The different displacement profiles of the 25 Hz actuation experiments causes a shift of the corresponding results compared to results obtained for all other actuation frequencies. Therefore, the results for 25 Hz do not follow closely the frequency trends of the other frequencies. We attribute these deviations to this methodological artifact and ignore them in the discussion section.

the same stress-strain offsets were applied in all data sets (3% strain and 2.85 MPa magneto-stress), Fig. 4b, c. Each stress-strain loop is an overlay of between 33 and 195 stress-strain loops, depending on the test frequency. The peak-to-peak strain for each test step was centered about the 3% starting strain. As test frequency increased, there was an increase in the magneto-stress with increasing peakto-peak strain. During the unloading portion of the cycle, the sample expanded and the stress-strain traces overlaid each other independent of strain rate. When cycling at higher frequency (e.g., 125 Hz, Fig. 4c), the stress hysteresis increased compared to cycling at lower frequency (e.g., 50 Hz, Fig. 4b). Dividing the work hysteresis area (which is the mechanical work density) by two times the peak-to-peak strain equals the average half width of the stress hysteresis, which is a measure for the dynamical twinning stress. Figure 4d shows the dynamical twinning stress as a function of frequency for different peak-to-peak strains. The dynamical twinning stress increased with increasing peak-to-peak strain and (above 50 Hz) with increasing frequency.

Mechanical work density per cycle ( $W_{\rm mechanical}$ , J/m<sup>3</sup>) was computed by integrating the stress strain curve using Eq. (2) for various peak-to-peak strain values (0.002, 0.005, 0.007, 0.009, 0.012, 0.016, 0.02, and 0.024) and test frequencies (25–150), Fig. 5. The mechanical work density increased monotonically with the peak-to-peak strain, it reached a maximum of 28.5 kJ/m<sup>3</sup> at the highest peak-to-peak strain (0.024) and 150 Hz, Fig. 5a. Below 0.016 peak-to-peak strain, the work density was constant and independent of test frequency, Fig. 5b. For frequencies above 100 Hz and 0.016 strain, the mechanical work density slowly increased with frequency. Mechanical work density increased as the peak-to-peak strain or the frequency increased.

Electrical work density per cycle ( $W_{\rm electrical}$ , J/m<sup>3</sup>) was computed by using Eq. (3), Fig. 6. Some of the data at high peak-to-peak strain and high frequency was omitted because the coil output voltage exceeded the analog input limit and the voltage was clipped (0.02–0.024 peak-to-peak strain and above 100 Hz). The logarithmic graph for electrical work density and peak-to-peak strain is linear with a slope of 1.9, Fig. 6a. Extrapolating from the electric work density results, a 0.024 peak-to-peak strain at 150 Hz yields nearly 20 J/m<sup>3</sup>, Fig. 6b.

Dividing the electrical work density (i.e., the output work density) by the mechanical work density (i.e., the input work density) yielded the work conversion efficiency, the power conversion efficiency of the inverse magnetoplastic effect (IMP) was computed, Fig. 7. The highest efficiency measured was 0.1% for 2.4% strain and 150 Hz, Fig. 7a, b.

For comparing our results with other results reported in the literature, the peak-to-peak voltage  $(V_{p-p})$  from the pickup coil and the electrical power  $(\mu W)$  was calculated, Fig. 8a, b. The electrical work density and the electrical power (Fig. 8b) from our results were calculated using  $V_{\rm rms}$  not  $V_{\rm p-p}$ . Analyzing the data it was found that:  $V_{\rm rms} \approx 0.3 V_{\rm p-p}$ . Since the electrical power is the square of the voltage, using peak-to-peak voltage overestimates the electrical power generated. Using  $V_{\rm rms}$  the maximum electrical power generated per cycle was 80  $\mu$ W at 150 Hz and 0.02 strain.

# Discussion

In "Results", we evaluated mechanical and electrical work densities and the conversion efficiency. Power densities are obtained from work densities by multiplication with frequency. Therefore, power and work conversion efficiencies are identical. Since power conversion efficiency is more commonly used for the generation of electrical energy, we use this term in the following discussion.

Equation (1) shows the voltage generated in the coil is proportional to the number of turns in the coil and the rate of change of magnetic flux through the coil. The area of the coil is constant, and  $\frac{d\phi}{dt} = A \frac{d\vec{B}}{dt}$ . The magnetic flux density  $\vec{B}$  is given by:

$$\vec{B} = \mu(\vec{M} + \vec{H}) = \mu_0(1 + \chi)\vec{H}.$$
 (4)

The magnetization is proportional to the fraction of each twin domain. Therefore, the change in flux is proportional to the rate of change of twin domain fraction in the sample. The magnetic dipole tied to the c-axis of 10 M Ni–Mn–Ga switches between parallel and perpendicular to the central axis of the coil; the magnetic susceptibility  $\chi$  changes drastically if the c-axis is parallel or perpendicular to the axis of the coil. This variation in  $\chi$  gives the induced electromagnetic field and voltage output.

The rate of change of the flux is proportional to the strain rate on the sample. The displacement can be described using a Fourier series with multiple terms of the form  $A\sin(\omega t + \varphi)$ , with amplitude A, frequency  $\omega$ , phase  $\varphi$ , and time t.

The electromotive force (and hence the induced voltage) is proportional to the rate of change of the flux density. The electrical power output is proportional to the square of the induced voltage, and, thus, the electrical power is proportional to the square of the actuation frequency in close agreement with experimental results (Fig. 6a, Carpenter et al. [6]). In contrast, the mechanical input power is the stress–strain hysteresis multiplied by the frequency. Since the hysteresis is constant (in the frequency range and strain



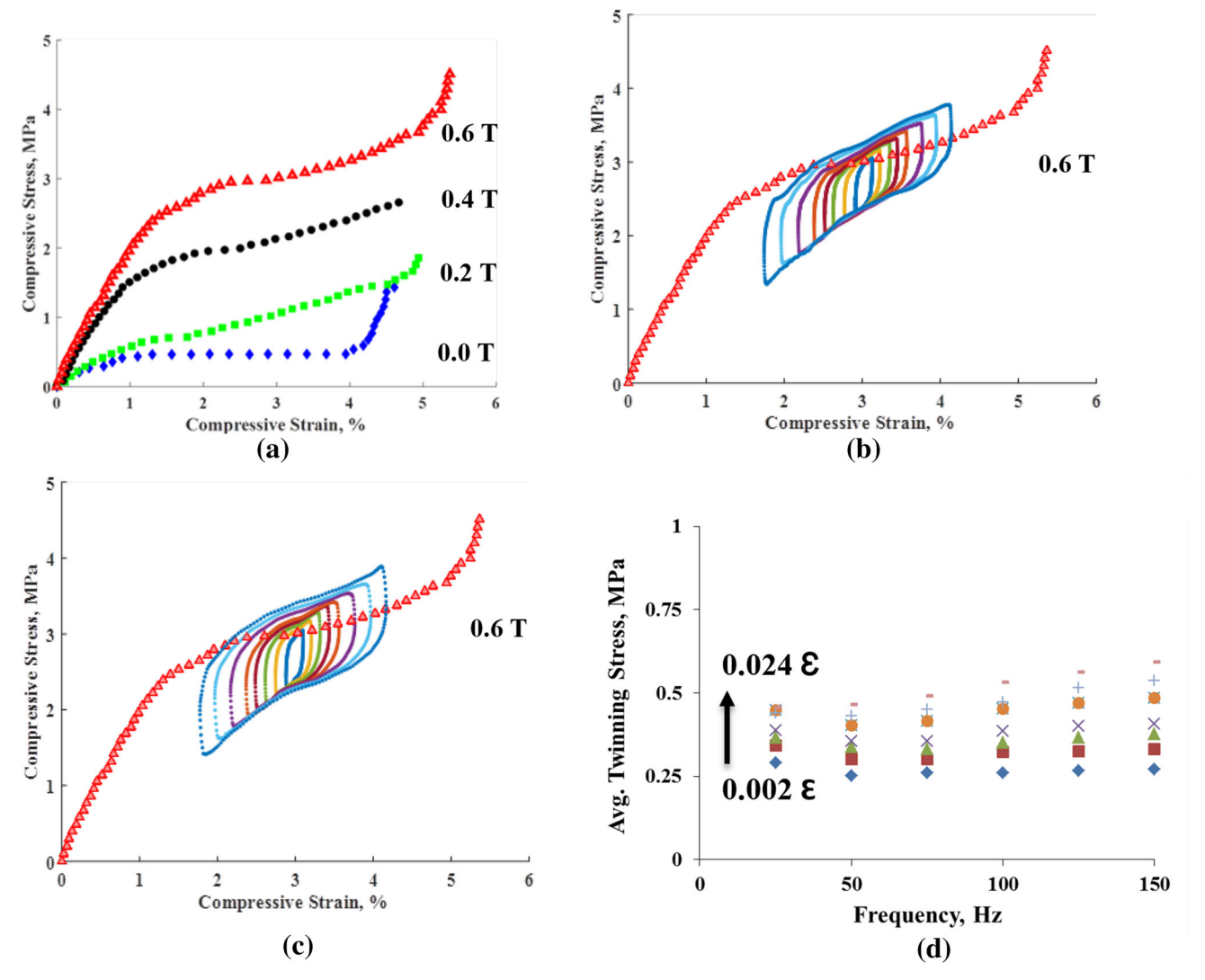


**Fig. 4 a** Quasi-static measurement of magneto-stress in compression at 0, 0.2, 0.4, and 0.6 T. The magneto-stress increased with increasing compressive strain when the magnetic field was on. **b** Stress-strain loops (65 cycles overlaid) while varying the peak-to-peak strain at 50 Hz and 0.61 T. **c** Stress-strain loops (166 cycles overlaid) while varying the peak-to-peak strain at 125 Hz and 0.61 T. As the

frequency and peak-to-peak strain increased, the compressive magneto-stress increased which led to an increased mechanical work density. **d** Average twinning stress for each frequency and peak-to-peak strain was calculated by dividing the mechanical work density by two times the peak-to-peak strain

range tested here, Fig. 5), the input power is proportional to the frequency (Fig. 7). Therefore, the efficiency (i.e., the ratio of output power and input power) is proportional to the actuation frequency.

For constant actuation frequency, the rate of change of twin fraction is proportional to the peak-to-peak strain. Hence, the output voltage is proportional to the peak-to-peak strain, whereas the output power is proportional to the square of the peak-to-peak strain. This is in good agreement with the slope 1.9 of the logarithmic electric work density versus strain plot. If the stress hysteresis was constant, the mechanical input work density would be proportional to the peak-to-peak strain. However, the stress hysteresis increases slightly with increasing peak-to-peak

strain. This behavior is consistent with the dependence of twin velocity on driving force reported by Faran et al. [14]. Therefore, the efficiency is under proportional to the peak-to-peak strain as seen in the slope of 0.66 in the logarithmic plot of efficiency and peak-to-peak strain. The mechanical input power depends linearly on the twinning stress. Therefore, the efficiency is inversely proportional to the twinning stress.

In the current experiments, a maximum efficiency of 0.1% was obtained at a frequency of 150 Hz, a peak-to-peak strain of 2.4%, and a twinning stress of 0.5 MPa. Following the argumentation set forth above, we estimate an efficiency of 20% for a Ni–Mn–Ga element with a twinning stress of 0.05 MPa, Straka et al. [15], operated at



Fig. 5 Mechanical work density varied with peak-topeak strain (0.002, 0.005, 0.007, 0.009, 0.012, 0.016, 0.020 and 0.024) and frequency (25-150 Hz). a Mechanical work density per cycle increased monotonically with peak-to-peak strain. b Below 0.16 peak-to-peak strain, the mechanical work density per cycle was constant with increasing frequency. Above 0.012 peak-to-peak strain and frequencies above 50 Hz mechanical work density slowly increased with frequency; also see Fig. 4b, c, d

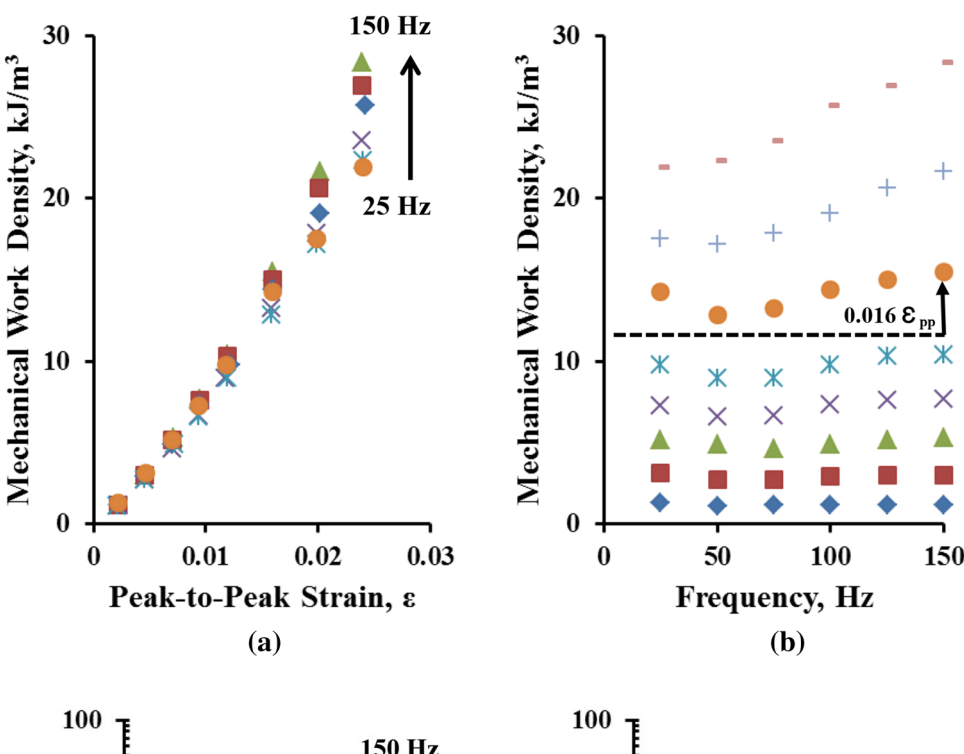
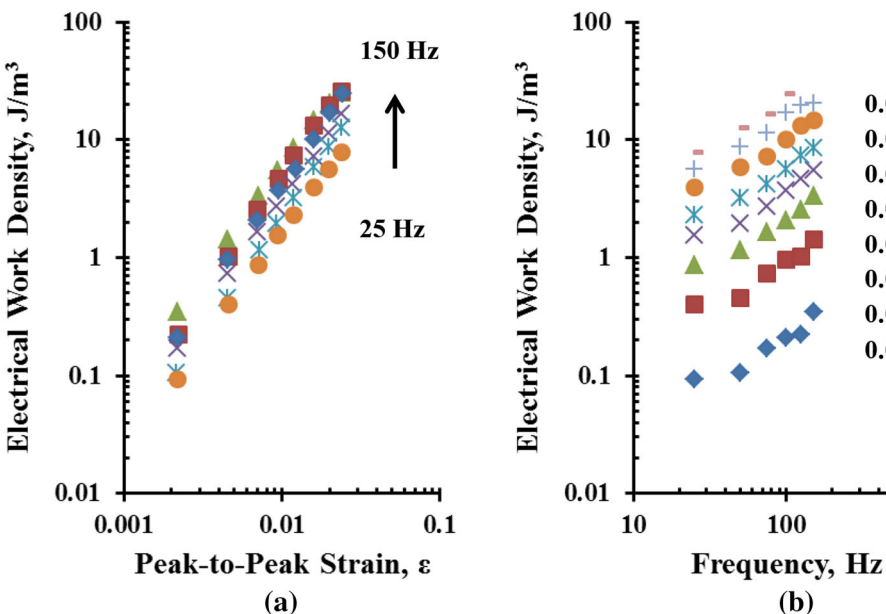


Fig. 6 a Log–log plot of electrical work density per cycle versus peak-to-peak strain with a slope of 1.93 for each data series and b electrical work density per cycle versus frequency. The maximum electrical work density was estimated as 30 J/m³ at 150 Hz and 0.024 peak-to-peak strain



a peak-to-peak strain of 7%, Pagounis et al. [16] and a frequency of 3 kHz.

At high frequencies, several phenomena limit the achievable efficiency. Faran and Shilo [14, 17] report that the driving force required for twin boundary motion increases substantially with increasing twin boundary velocity. Assuming that a single twin boundary moves through the sample, the required twin boundary velocity is proportional to the frequency, the sample size, and the peak-to-peak strain. For the present sample (length 6.46 mm, actuation frequency 150 Hz, peak-to-peak strain 2.4%), this implies a twin boundary velocity of 0.4 m/s.

Even for the high mobility type II twin the twinning stress exceeds 0.1 MPa for twin boundary velocities exceeding 1 m/s [14]. The increased twinning stress increases the stress hysteresis and the mechanical work input, and, thus, reduces the efficiency. This effect is seen in our data in the frequency dependence and the peak-to-peak strain dependence of the dynamical twinning stress (Fig. 4d).

To reduce the twin boundary velocity, one may introduce a high number of twin boundaries. However, methods that stabilize a dense twin microstructure also increase the twinning stress Chmielus et al. [18]. Therefore, the potential to enhance efficiency through a high number of



0.024 ε

0.020 4

0.016

0.012

0.009

0.007 0.005 0.002 ε

1000

Fig. 7 a Log-log plot of the power conversion efficiency versus peak-to-peak strain and b log-log plot of the power conversion efficiency versus test frequency

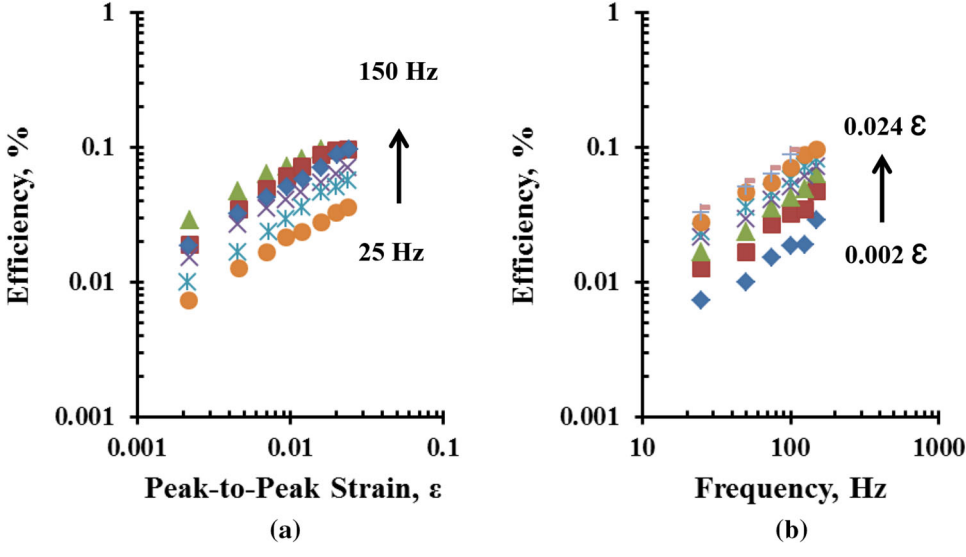
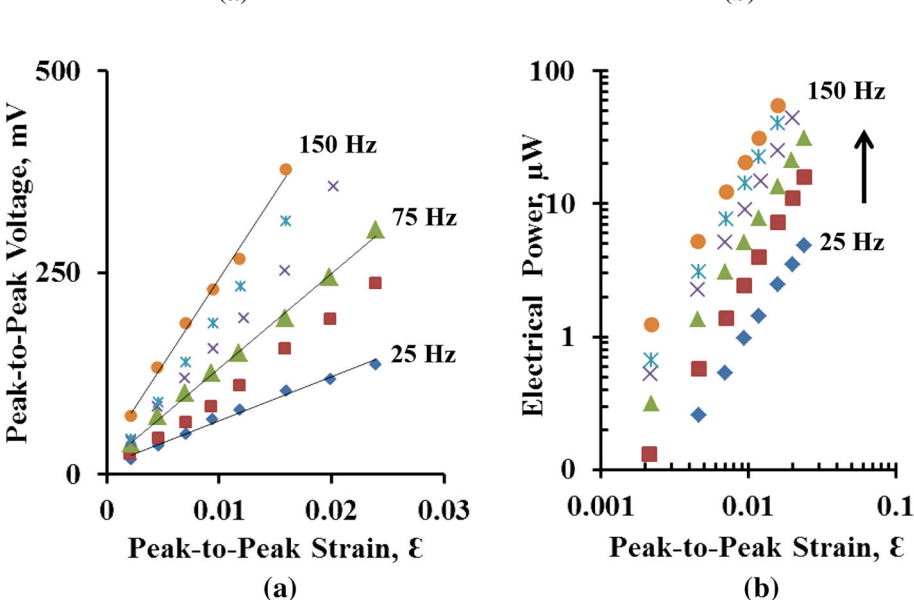


Fig. 8 a The peak-to-peak voltage instead of  $V_{\rm rms}$  was used to compare these results with those of other researchers. For our results, peak-to-peak voltage was three times higher than the  $V_{\rm rms}$ . b The electrical power,  $\mu$ W, calculated for this study from 25 to 150 Hz using the  $V_{\rm rms}$  not the  $V_{\rm p-p}$ . The maximum power was near 100  $\mu$ W at 150 Hz and 0.024 peak-to-peak strain



twin boundaries is limited. The required twin velocity decreases with decreasing sample size. Musiienko et al. [19] report a weak dependence on size of magnetic and magneto-mechanical properties down to a sample thickness of 1  $\mu$ m. Thus, the efficiency may be increased to some extent for smaller samples.

Lastly, at high frequency, eddy currents may reduce the efficiency (a) through self-induction and (b) through heating. Gaitzsch et al. [20] noticed a temperature increase of a few degrees through eddy currents when rotating a field of 0.97 T at 4000 rpm (67 Hz). In those experiments, the magnetic flux density variation was about one order of magnitude larger than in the experiments presented here. Thus, eddy current heating is expected here at a ten times higher frequency, i.e., above 600 Hz. Eddy currents are reduced in samples of smaller size and heating through eddy currents may be less severe at smaller scale. Thus,

small samples may in fact provide higher energy conversion efficiencies than large samples.

## **Conclusions**

We analyzed experimentally the conversion of mechanical to electrical power through a magnetic shape memory alloy transducer located in the core of a 1601 winding pickup coil. The power conversion efficiency increases with (i) increasing actuation frequency, (ii) increasing actuation stroke, and (iii) decreasing twinning stress. Extrapolating from the results of low-frequency experiments to the kHz actuation regime yields a power conversion frequency of about 20% for 3 kHz actuation frequency, 7% actuation strain, and 0.05 MPa twinning stress. At high frequency, the kinetic properties of twin boundaries and Joule heating



through eddy currents reduce the achievable efficiency. These diminishing effects are less effective in small transducers. We expect high-energy transformation efficiency for high frequency sources and small transducer size.

Acknowledgements The authors thank Professors Nader Rafla and John Chiasson of the Department of Electrical and Computer Engineering at Boise State University for their technical advice during the project; mechanical engineering undergraduate students, Sam Barker and Eric Rhoades for their assistance designing and building the magneto-mechanical test apparatus; graduate student Theodore Lawrence for his assistance characterizing the composition, structure, and transformation temperatures of the samples. We acknowledge partial financial support from the National Science Foundation through Grant DMR-1710640.

#### References

- Suorsa I, Tellinen J, Ullakko K, Pagounis E (2004) Voltage generation induced by mechanical straining in magnetic shape memory materials. J Appl Phys 95(12):8054–8058
- Karaman I, Basaran B, Karaca HE, Karsilayan AI, Chumlyakov YI (2007) Energy harvesting using martensite variant reorientation mechanism in a NiMnGa magnetic shape memory alloy. Appl Phys Lett 90(17):172505
- Marioni M, O'Handley RC, Allen SM (2003) Pulsed magnetic field-induced actuation of Ni-Mn-Ga single crystals. Appl Phys Lett 83(19):3966–3968
- Müllner P, Chernenko VA, Kostorz G (2003) Stress-induced twin rearrangement resulting in change of magnetization in a Ni-Mn-Ga ferromagnetic martensite. Scripta Mater 49(2):129–133
- Li G, Liu Y, Ngoi BKA (2005) Some aspects on strain-induced change of magnetization in a Ni-Mn-Ga single crystal. Scripta Mater 53:829–834
- Carpenter D, Chmielus M, Rothenbühler A, Schneider R, Müllner P (2009) Application of ferromagnetic shape memory alloys in power generation devices. In: Olson GBL, Saxena DS, (eds) ICOMAT-08, Santa Fe, NM, pp 365–369
- Bruno NM, Ciocanel C, Feigenbaum HP, Waldauer A (2012) A theoretical and experimental investigation of power harvesting using the NiMnGa martensite reorientation mechanism. Smart Mater Struct 21:1–12

- Nelson I, Ciocanel C, LaMaster D, Feigenbaum HP (2013) Three dimensional experimental characterization of NiMnGa alloy. In: Goulbourne NC, Naguib HE (eds) Behavior and mechanics of multifunctional materials and composites. SPIE, Bellingham
- Guiel R, Dikes JL, Ciocanel C, Feigenbaum HP (2015) Further insight on the power harvesting capabilities of magnetic shape memory alloys. In: Conference on smart materials, adaptive structures and intelligent systems. ASME, Colorado Springs, Colorado
- Lindquist PG, Müllner P (2015) Working Ni-Mn-Ga single crystals in a magnetic field against a spring load. Shap Mem Superelasticity 1(1):69–77
- Hobza A, Patrick C, Ullakko K, Rafla N, Lindquist P, Müllner P (2018) Sensing strain with Ni-Mn-Ga. Sensor Actuat a-Phys 269:137–144
- Analog Devices, "Universal LVDT Signal Conditioner", AD 698 Data Sheet, 1995 [rev. C]
- Kellis D, Smith A, Ullakko K, Müllner P (2012) Oriented single crystals of Ni-Mn-Ga with very low switching field. J Cryst Growth 359:64–68
- Faran E, Shilo D (2012) Implications of twinning kinetics on the frequency response of NiMnGa actuators. Appl Phys Lett 100(151901):1–4
- Straka L, Drahokoupil J, Pacherova O, Fabianova K, Kopecky V, Seiner H, Hänninen H, Heczko O (2016) The relation between lattice parameters and very low twinning stress in Ni50Mn25 + xGa25-x magnetic shape memory alloys. Smart Mater Struct 25(2):025001 (2016)
- Pagounis E, Laptev A, Jungwirth J, Laufenberg M, Fonin M (2014) Magnetomechanical properties of a high-temperature Ni-Mn-Ga magnetic shape memory actuator material. Scripta Mater 88:17–20
- Faran E, Shilo D (2011) The kinetic relation for twin wall motion in NiMnGa. J Mech Phys Solids 59:975–987
- Chmielus M, Witherspoon C, Ullakko K, Müllner P, Schneider R (2011) Effects of surface damage on twinning stress and the stability of twin microstructures of magnetic shape-memory alloys. Acta Mater 59:2948–2956
- Musiienko D, Saren A, Ullakko K (2017) Magnetic shape memory effect in single crystalline Ni-Mn-Ga foil thinned down to 1 um. Scripta Mater 139:152–154
- Gaitzsch U, Romberg J, Pötschke M, Roth S, Müllner P (2011)
  Stable magnetic-field-induced strain above 1% in polycrystalline
  Ni-Mn-Ga. Scripta Mater 65:679–682

